Title

Ultrasound molecular imaging of tumor angiogenesis with a neuropilin-1-targeted microbubble



Authors

Zhang, Hua
Tam, Sarah
Ingham, Elizabeth S
et al.

Publication Date

2015-07-01

DOI

10.1016/j.biomaterials.2015.03.043

Peer reviewed

HHS Public Access

Author manuscript

*Biomaterials*. Author manuscript; available in PMC 2016 July 01.

Published in final edited form as:

*Biomaterials*. 2015 July ; 56: 104–113. doi:10.1016/j.biomaterials.2015.03.043.

# Ultrasound Molecular Imaging of Tumor Angiogenesis with a Neuropilin-1-Targeted Microbubble

**Hua Zhang**[*], **Sarah Tam**[*], **Elizabeth S. Ingham**[*], **Lisa M. Mahakian**[*], **Chun-Yen Lai**[*], **Spencer K. Tumbale**[*], **Tambet Teesalu**[~], **Neil E. Hubbard**[^], **Alexander D. Borowsky**[^], and **Katherine W. Ferrara**[*]

[*]Department of Biomedical Engineering, University of California, Davis, California, 95616

[^]Center for Comparative Medicine, University of California, Davis, California, 95616

[~]Sanford-Burnham Medical Research Institute, La Jolla, CA 92037

## Abstract

Ultrasound molecular imaging has great potential to impact early disease diagnosis, evaluation of disease progression and the development of target-specific therapy. In this paper, two neuropilin-1 (NRP) targeted peptides, CRPPR and ATWLPPR, were conjugated onto the surface of lipid microbubbles (MBs) to evaluate molecular imaging of tumor angiogenesis in a breast cancer model. Development of a molecular imaging agent using CRPPR has particular importance due to the previously demonstrated internalizing capability of this and similar ligands. *In vitro*, CRPPR MBs bound to an NRP-expressing cell line 2.6 and 15.6 times more than ATWLPPR MBs and non-targeted (NT) MBs, respectively, and the binding was inhibited by pretreating the cells with an NRP antibody. *In vivo*, the backscattered intensity within the tumor, relative to nearby vasculature, increased over time during the ~6 min circulation of the CRPPR-targeted contrast agents providing high contrast images of angiogenic tumors. Approximately 67% of the initial signal from CRPPR MBs remained bound after the majority of circulating MBs had cleared (8 min), 8 and 4.5 times greater than ATWLPPR and NT MBs, respectively. Finally, at 7–21 days after the first injection, we found that CRPPR MBs cleared faster from circulation and tumor accumulation was reduced likely due to a complement-mediated recognition of the targeted microbubble and a decrease in angiogenic vasculature, respectively. In summary, we find that CRPPR MBs specifically bind to NRP-expressing cells and provide an effective new agent for molecular imaging of angiogenesis.

### Keywords

Molecular Imaging; Angiogenesis; Peptide; Targeting; Microbubble; *in vivo*



Corresponding Author: Katherine W. Ferrara PhD, Department of Biomedical Engineering, University of California, Davis, 451 Health Sciences Drive, Davis, California 95616, Phone: +1 (530) 754-9436, Fax: +1 (530) 754-5739, kwferrar@ucdavis.edu.

## Introduction

Ultrasound (US) molecular imaging combines many advantages of US imaging, including low cost, non-invasive and real-time protocols, with the opportunity to assay vascular receptor expression. To accomplish US molecular imaging, microbubble contrast agents are coated with targeting ligands and are injected into the vascular space [1–3]. Microbubble contrast agents circulate within the vasculature for minutes providing the opportunity to survey vascular surface receptors without a confounding signal from an extravasated imaging probe. Here, with two neuropilin-1 (NRP)-targeted peptides, we constructed two NRP-targeted microbubbles (MBs), established optimized US parameters for molecular imaging and compared the performance of the targeted MBs with non-targeted (NT) MBs both *in vitro* and *in vivo*.

NRP has been identified as an isoform-specific receptor for vascular endothelial growth factor [4] and its expression is up-regulated in multiple tumor types as well as on tumor vasculature [5–8]; therefore, NRP-based molecular imaging can be used as an indication of local angiogenesis. Recently, peptides containing a C-terminal arginine with a free carboxyl group (CendR) were shown to target NRP [9], and two peptides, ATWLPPR (abbreviated as ATW in this paper) [10] and CRPPR (abbreviated as CRP in this paper) [11], were reported as CendR peptides binding to NRP. Further, CendR peptides, and CRPPR in particular, have been shown to enhance the internalization of their cargo and are therefore particularly important targets for tumor drug delivery [11]. Such peptides are also hypothesized to be produced at the tumor site by enzymes acting upon circulating internalizing RGD (iRGD) peptides [12]. Therefore, the creation of an imaging probe capable of assaying NRP receptors that are accessible on tumor vasculature has the potential to facilitate personalized treatment based upon the iRGD or CendR strategy.

In this paper, we conjugated lipids, polyethylene glycol and the ATW or CRP peptides to form lipo-PEG-peptides that were then incorporated with other lipids into targeted MBs. A major advantage of peptide targeting and the lipo-PEG-peptide strategy employed here is a reduction in immunogenicity as compared with antibodies and biotin-avidin conjugation. However, we have previously shown that the incorporation of an exposed peptide on the relatively large surface of a microbubble has the potential to enhance the attachment of C3/C3b and production of soluble C3a anaphylotoxin [13]. Repeated imaging over a duration of several days to weeks is also often required to optimize a tumor model [14], to study biological changes with tumor growth [15] or to evaluate anti-angiogenic therapy [16]. Few studies have evaluated the effect of repeated MB injections on imaging. Therefore, we assess whether repeated microbubble administration affects the circulation or accumulation.

Our central goal is to design a strategy to use US molecular imaging to assess the local NRP concentration and detect small tumors with high sensitivity. In nuclear medicine, the relative accumulation of molecularly-targeted contrast agents is quantified and the receptor kinetics are modeled to facilitate comparisons of performance [17–19]. Ultrasound contrast agents are multi-valent constructs that rapidly accumulate on the vascular surface and are not typically characterized by classical receptor kinetics. Still, quantification of the rate of accumulation provides an effective scheme to compare molecularly-targeted microbubbles.

Blood flow has been reported to be reduced for up to 40 min within tumor vasculature after insonation of targeted, but not NT MBs, with a high frequency (5 MHz) and high peak-negative pressure (PNP) (2 or 4 MPa) [20]. With a higher PNP and lower center frequency, similar effects have been reported for non-targeted MBs [21–23]. The hypothesized mechanism was the oscillation and collapse of MBs mechanically disrupting a limited number of endothelial cells, which can expose the basement membrane and recruit platelets to the site. A reduction in blood flow is undesirable as multiple targeted MB injections are often required within a single imaging session to study short-term biological changes, to optimize system parameters or to evaluate novel MB formulations [24, 25]. Therefore, we seek the ideal insonation parameters that facilitate quantitative imaging but do not result in significant biological effects in order to facilitate the incorporation of this new imaging probe into pre-clinical and clinical studies.

## Materials and Methods

All reagents, including solvents, amino acids, Fmoc-Peg27-OH and Fmoc-Arg(Pbf)-Wang resin, were purchased from EMD Biosciences (La Jolla, CA) unless otherwise specified. Lipids, disteroylphosphatidylcholine (DSPC) and 1,2-distearoyl-sn-glycero-3-phosphoethanolamine-N-[methoxy(polyethylene glycol)-2000] (ammonium salt) (DSPE-PEG2K), were purchased from Avanti Polar Lipids (Alabaster, AL). Complement-preserved human serum was purchased from Valley Biomedical (cat. no. HC1004, Winchester, VA). Serum was thawed and/or stored on ice prior to experiments.

### Lipo-Peg-Peptide (LPP) synthesis

Two CendR [9] peptides, ATWLPPR [10] and CRPPR [11], were synthesized with standard Fmoc protocol [26] on a Biotage® Initiator+ Microwave Synthesizer (Biotage, Charlotte, NC), with Fmoc-Arg(Pbf)-Wang resin used to produce carboxylic acid at the C-terminus. After the two Fmoc-peptides were synthesized on the resin, a small amount of Fmoc-peptide was cleaved from the resin and the mass was checked with MALDI (ABI-4700 TOF-TOF, Applied Biosystems, Foster City, CA): Fmoc-ATWLPPR, expected 1061.55, measured ($H^+$) 1062.68; Fmoc-CRPPR, expected 849.40, measured ($H^+$) 849.66. The two peptidyl resins were then coupled with PEG and lipids on resin, as described in [27]. The two LPPs were then cleaved from the resin and purified with RP-HPLC, and the molecular weights were further assessed with MALDI (ATW LPP, expected 5410.41, measured ($H^+$) 5412.19; CRP LPP, expected 5198.25, measured ($H^+$) 5194.31). The CRP LPP was further dimerized with air and the dimer was purified with RP-HPLC, as described in [27].

### MB Preparation

The lipids and LPPs were mixed in chloroform (Sigma-Aldrich, St. Louis, MO), and the chloroform was blow-dried under a gentle nitrogen gas stream and thoroughly vacuumed on the lyophlizer overnight. MB buffer was made by mixing 0.9% sodium chloride (B. Braun Medical Inc., Irvine, CA), propylene glycol (Sigma-Aldrich, St. Louis, MO), and glycerol (MP Biomedicals, LLC) with the ratio of 80:10:10 (v/v/v), and the pH was adjusted with sodium hydroxide to 7.4. The dried lipid mixture was re-suspended with degassed MB buffer by first warming in a water bath (60–65°C for 15 min), and then sonicating (60–65°C

for 15 min) until all of the lipids were re-suspended in a clear solution of 2.5 mg per ml. After being cooled to room temperature, the liposome solution was aliquoted into 2ml serum glass bottles (VWR, Visalia, CA), containing 1.0 ml per bottle. After sealing the bottle, the air in the bottle headspace was purged with 10 ml perfluorobutane $C_4F_{10}$ (FluoroMed, L.P., Round Rock, TX), and the resulting liposome solutions were kept at 4°C until use.

MBs were activated by shaking on a Vialmix (Lantheus Medical Imaging, North Billerica, MA), and purified by centrifugation, similar to [28], as detailed below. The activated MBs suspension was collected into a 3 ml syringe (Covidien, Mansfield, MA), which was further filled with degassed Dulbecco's phosphate-buffered saline (DPBS, Mediatech, Inc. Manassas, VA). Centrifugation (10 min, 300 RCF) was performed to collect the MBs into a cake resting against the syringe plunger. After removing the infranatant, the bubble cake was re-suspended with 2.5 ml DPBS. MBs larger than 10 μm were removed by centrifugation: 16 RCF for 1 min, followed by 45 RCF for 1 min, in which the infranatant was collected. MBs smaller than 1 μm were removed by 3 times centrifugation (300 RCF for 3 min), in which the infranatant was removed and the bubble cake was collected. For *in vitro* tests, the steps involved in removing MBs larger than 10 μm were omitted. The size and concentration of the MBs were measured with an Accusizer 770A (Particle Sizing Systems, Port Richey, FL), and the MBs were used within 3 hours after shaking.

## Cell culture

While the *in vivo* imaging target for microbubbles is the angiogenic endothelium, a NRP-expressing tumor cell line, primary prostate carcinoma-1 (PPC-1) was used to assess *in vitro* binding as the expression of NRP on this cell line is well established and endothelial expression varies between *in vitro* and *in vivo* assays [11]. The PPC-1 cell line was a generous gift from Dr. Arthur Brothman (University of Utah, School of Medicine), and was cultured and maintained using DMEM high glucose media (Invitrogen, Carlsbad, CA) supplemented with 1% Penicillin-Streptomycin (10,000U/ml, Invitrogen, Carlsbad, CA) and 10% fetal bovine serum (Omega Scientific Inc., Tarzana, CA). For MB binding experiments, PPC-1 cells were plated onto collagen-coated 25-mm glass coverslips the day before experiments, followed by incubation at 37°C in a humidified tissue culture incubator 95%/5% air/$CO_2$ to reach a confluency of 95% on the day of experiments.

## *In vitro* MB binding and inhibition study

MB binding was tested following a procedure similar to [29], and described briefly here. A glass coverslip with a PPC-1 cell mono-layer was mounted in a stainless steel holder to provide a frame with a 2-mm deep well above the cell layer (Supplementary Figure 1). After 1 ml of MB suspension (with 2 or $5 \times 10^7$ MB/ml) in DPBS was added into the well, the well was covered with a 35-mm glass coverslip to retain the liquid in the well, then inverted and maintained at 37°C for 5 min to allow MBs to rise via buoyancy to the cell plate. The well was then flipped back to its original position, the 35-mm coverslip was removed, and the cell layer was gently rinsed with DPBS 3 times to remove unbound MBs. The cell plate was imaged on a custom upright microscope (Mikron, San Marcos, CA) with a digital Cascade 512b camera (Photometrics, Tucson, AZ) using bright field imaging with a 63× water-immersion objective (Achroplan, Zeiss, NY) driven with SimplePCI 6 software. For

each condition, 4–5 plates of cells were tested (n = 4–5). Five images were acquired randomly per plate and analyzed with ImageJ (imagej.nih.gov/ij/), and the MB area per field of view was calculated from the “Analyze Particle” function in ImageJ.

For the inhibition study, an anti-NRP antibody was generated as in [9]. Glass coverslips with PPC-1 cell monolayers were incubated with NRP antibody solution (20 μg/ml) at 37°C for 30 min prior to the MB treatments described above.

## Overview of the *in vivo* studies

All animal studies were conducted under a protocol approved by the University of California, Davis Animal Care and Use Committee. Female FVB mice, 5–6 weeks old, 15–25 g, were purchased from Charles River Laboratory International Inc. (Wilmington, MA). Tumors were grown by transplanting one 1 $mm^3$ piece of donor NDL tumor into each of the two 4th mammary fat pads, and allowing the tumors to grow for 3 weeks before imaging [30], at which time the tumors were 2–3 mm in longitudinal diameter.

Before MB imaging, mice were anesthetized with 2% isoflurane (Halocarbon Laboratory, River Edge, NJ) in oxygen (2 L/min) and placed on a heated stage to maintain body temperature at 37°C. The skin above and around the tumor was shaved and further treated with depilatory (Veet, Reckitt Benckiser) to fully remove all fur, and ultrasound gel (Aquasonic, Parker Laboratories Fairfield, NJ) was applied to couple the ultrasound transducer. MBs were administered by tail vein injection with a 27-gauge needle connected to a cannula. A dose of MB in 50 μl saline was injected followed by a 10 μl saline flush. The number of consecutive injections per imaging session was limited to 4 or less, to minimize the time under anesthesia and the volume of fluid injected.

## Statistical methods

The N numbers of each study is summarized in the table below. Based on previous experience, N=3 is sufficient to confirm the acoustical parameters required for imaging and destruction as there is little variability. For studies with variability based on the tumor biology (e.g. targeted microbubble accumulation), a minimum of N=4 has been sufficient. For longitudinal studies or studies of antibody inhibition, a larger cohort is required in order to insure significance (N=6 or greater). The cohort size is summarized below.

| | **N** |
|---|---|
| MBD parameter optimization | 3 |
| *In vivo* MB binding comparison | 4 |
| *In vivo* MB binding inhibition | 7 |
| Effect of repeated CRP MB injection | 6(Day 0–14); 5 (Day 21) |

All data are presented as mean ± standard deviation from 3 or more replicates, calculated in Excel 2010. All of the multiple comparison statistics were performed with GraphPad Prism 6.0, with Tukey’s (or Dunnett’s) multiple comparison correction. A p value smaller than 0.05 was considered to be significant. One-way ANOVA with Tukey’s multiple

comparisons correction was performed to test the significance during microbubble parameter optimization. Paired one-way ANOVA with Dunnett's multiple comparisons correction was performed to test the significance between the first and the later microbubble injections.

### Microbubble destruction (MBD) parameter optimization

MBD parameters were optimized by studying the effect of PNP (0.5, 1, 2MPa) and duration (1, 2s) on US signal, blood flow, and tumor binding. To test whether MBD parameters were effective, mice were injected with $1 \times 10^8$ NT MBs, and MBD was applied between 30 sec and 2 min post injection. A 10 sec clip was recorded 3 sec before MBD, and the US signal intensity after MBD was normalized by the US signal intensity immediately prior to MBD (n=3).

The effect of repeated injection/MBDs on blood flow was characterized by the tumor US signal intensity at 30 sec post injection, normalized by the value from the first injection. The effect of repeated injection/MBD on MB binding was characterized by the tumor US intensity change caused by MBD at 8min, after being normalized by the tumor intensity at 30 sec post injection. Mice were injected with $5 \times 10^7$ CRP MBs (n=3 for each condition), with MBD applied at 8.25 min. Clips of 10 sec were recorded at 0.5, 8, and 8.5 min post injection and the procedure was repeated 4 times.

### Imaging protocol

Ultrasound imaging was performed as in [20, 31], with some modifications. Contrast pulse sequencing (CPS) contrast imaging mode (Sequoia 512; Siemens, Issaquah, WA; 15L8 transducer, center frequency of 7 MHz) was used to visualize both flowing and bound MBs. CPS imaging parameters remained constant through this paper: a Mechanical Index (MI) of 0.09 (PNP of 230 kPa), a frame rate of 11 Hz, and a CPS gain of −12 dB. For each MB injection, a B mode image was acquired before injection to locate the tumor, and CPS clips of 10 sec in duration were acquired immediately before injection, at the time of injection (0 min), and 0.5, 1, 2, 4, 6, 8, 8.25, and 8.5 min post injection. A microbubble destruction (MBD) pulse was applied at 8.25 min to destroy the MBs.

### Specificity of MB tumor accumulation

To compare the *in vivo* performance of CRP, ATW, and NT MBs, four tumors (n = 4) were injected with $5 \times 10^7$ CRP, ATW, and NT MBs consecutively in a random order and imaged after each MB injection. To study the specificity of CRP MB's binding, 7 tumors (n = 7) were imaged after CRP MB injection to assess baseline MB adhesion, followed by injection of NRP antibody (50 μg per mouse), and 30 min later CRP MBs were injected again and the tumors were imaged. The larger number (n=7) was required to characterize the effect of the antibody. CD31 staining of the vasculature was added to formalin-fixed tumor sections as in [32] and the area of staining was quantified using Image J. NRP staining of the vasculature was performed using an anti-NRP antibody (AB81321, Abcam, Cambridge, England) according to the procedure specified by the manufacturer.

### Effect of repeated CRP MB injections

To study the effect of repeated CRP MB injections, 6 mice were injected with $5 \times 10^7$ CRP MB on Day 0, 1, 7, and 14, and imaged afterwards. On Day 21, 5 mice survived and were injected with MB and imaged as in the earlier studies.

### Human complement C3 binding to the microbubble surface

Microbubbles were diluted in a syringe to $2\times10^9$ per mL in 2 mL PBS and mixed with 0.6 mL serum. The mixture was incubated on a benchtop rotator at room temperature for 30 min. After incubation, the mixture was centrifuged at 300 g for 3 min to isolate microbubbles. The microbubble cake was re-suspended into PBS and washed three times. Microbubbles were then mixed with a 2mL solution (25 mg/mL) of fluorescently-tagged antibody to human C3/C3b (CL2103F, Cedarlane, Hornby, Ontario), incubated for 30 min, and washed three times. Median fluorescence intensity per microbubble was determined by FACScan flow cytometry (Becton Dickinson, Franklin Lakes, NJ).

### US image analysis

All of the US images were recorded digitally and analyzed offline with MATLAB (Mathworks, Natick, MA) and ImageJ. Motion correction was performed on each 10-sec clip, and the aligned CPS images were averaged on a pixel-by-pixel basis, as detailed in [31]. Quantitative image intensity measurements were then made over manually selected regions of interest (ROI) on the averaged images. The image intensity was normalized by the peak intensity measured at 30 sec after MB injection, to account for potential variation in injected contrast volume or vascular delivery of MBs to the tumor. Digital subtraction of the postdestruction average image was also applied to predestruction average images to evaluate the contribution of MBD pulses to the differentiation of free and bound MBs.

## Results

### Effects of ligand percentage on MB stability

Typical size distributions of MBs with 0–5 % of CRP LPP incorporated in the MB lipid shell are shown in Fig. 1A–D, with arrows pointing to the direction of increasing CRP LPP percentage. Compared with the NT MBs (X=0), MBs with 1% CRP LPP were slightly larger (however, not statistically significant) both in number-weighted (Fig. 1A, C) and volume-weighted (Fig. 1B, D) size distribution curves. MBs with 3% or 5% CRP LPP had broader size distributions (Fig. 1B, D), where a peak between 3 and 10 μm increased with the percentage of the CRP LPP. As a result, the number-weighted mean diameter did not change, while the volume-weighted mean diameter increased with the percentage of CRP LPP (Fig. 1E). Further, the total number of MBs produced decreased with an increasing percentage of CRP (Fig. 1F). We hypothesize that the larger size and smaller number of MBs indicate that the ligand interaction forms larger MBs and decreases MB stability with 3 or 5% CRP on the lipid shell. Therefore, in the remainder of this paper, the ligand percentage was set as 1%.

### Binding to NRP-expressing cells

The MB's affinity to NRP was tested on an NRP-expressing cell line, PPC-1 [11], and the binding specificity was confirmed by a blocking study with the NRP antibody [9] (Fig. 2). CRP MBs bound 2.6 and 15.6 times more than ATW MBs and NT MBs, respectively, at a concentration of $2 \times 10^7$ MBs/ml, and 1.9 and 32.8 times more than ATW MB and NT MB at a concentration of $5 \times 10^7$ MBs/ml. The binding of CRP MBs was specific to NRP: pre-incubating the cells with NRP antibody decreased binding to 4% and 39% at $2 \times 10^7$ and $5 \times 10^7$ MB/ml, respectively.

### MBD setting

While consecutive repeated injections were desired to compare the performance of CRP MBs, ATW MBs and NT MBs *in vivo*, earlier research in our lab has found that MBs insonified with a 2 MPa or 4 MPa PNP at a frequency of 5MHz transiently decreased blood flow [20]. Therefore, we first optimized MBD parameters to minimize these bio-effects. More than 50% of the MB signal intensity remained after MBD with 0.5 MPa, while MBD with 1 or 2 MPa decreased the signal to less than 10% of the original value (Fig. 3A). As 2 MPa MBD decreased blood flow, we studied the effect of a lower amplitude MBD pulse (1 MPa and 1 sec) on blood flow, by repeating cycles of injection and MBD (at 8.25 min post injection), and comparing the tumor signal intensity at 30 sec post injection to the value of the first injection. Blood flow was not affected for up to 3 repetitions of CRP MB injection and destruction; at the fourth injection, the circulating echoes decreased to 77.9% ($p = 0.42$) of that recorded with the first injection (Fig. 3B). We then evaluated the influence of repeated injection/MBDs on MB binding (Fig. 3C) by calculating the tumor intensity difference before and after MBD ("before MBD" contains bound and circulating MBs, "after MBD" contains circulating MBs only). Within the scope of this study, no significant change was observed after 4 repeated cycles of injection and MBD. Therefore, 1 MPa and 1 sec were chosen as the MBD parameters used in all *in vivo* studies, and the number of consecutive targeted MB injections was limited to 3 for each animal to avoid possible bio-effects.

### *In vivo* MB binding study

*In vivo* US images demonstrate that CRP MBs bound to NDL tumors (Fig. 4, A –F) at a greater rate than ATW MBs (Fig. 4G–L) and NT MBs (Fig. 4M–R). Quantification was performed on the tumor and a nearby blood vessel to study the tumor binding kinetics and blood clearance (Fig. 5). Echoes from CRP MBs in tumors decreased more slowly than echoes from ATW and NT MBs (Fig. 5A). At 8 min after injection, 73.0% ± 14.1% of the initial signal remained for CRP MBs while 11.1% ± 3.9%, 26.1% ± 18.0% of the initial signal remained for ATW and NT MBs, respectively. An MBD pulse at 8.25 min further differentiated the circulating MBs and bound MBs. At this time, 67.0% ± 12.2% of the initial signal for CRP MBs resulted from bound MBs, 8.0 and 4.5 times higher than ATW and NT MBs, respectively (Fig. 5B). Contrary to the different kinetics in the tumor, the CRP MBs and NT MBs have similar blood clearance profiles, each circulating longer than ATW MBs (Fig. 5C and D). The normalized intensity difference between the tumor and vessel increases over time for CRP MBs, but not for ATW or NT MBs (Fig. 5E), with an area

under the curve of 3.6 min for CRP MB, which was 7.6 and 15 times greater than ATW and NT MBs, respectively (Fig. 5F).

Similar to the *in vitro* results, pre-administration of an NRP antibody decreased CRP MB binding to the NDL tumor vasculature, characterized by the normalized intensity difference before and after MBD (Fig. 5G). Pre-administration of the NRP antibody decreased the difference from 0.58 ± 0.10 to 0.36 ± 0.10, $p = 0.007$.

### Accelerated clearance

Finally, we studied the effects of repeated CRP MB injection on the signal kinetics in the tumor and blood vessels over a period of 21 days (Fig. 6). The CPS image intensity on Day 1 was similar to that observed on Day 0 (Fig. 6A) and was significantly decreased upon a third injection on Day 7 (Fig. 6B). Both the tumor accumulation (Fig. 6C, 6E) and the blood circulation of the MBs (Fig. 6D, 6F) were decreased upon injections on Days 7, 14 and 21. The tumor accumulation of targeted MBs, which occurred on Day 0 and Day 1 but was not observed on Day 7, was observed in 2 of 6 tumors on Day 14 and 2 out of 6 tumors on Day 21.

In order to determine whether the reduced accumulation resulted from reduced angiogenesis, we evaluated CD31 and NRP stains via immunohistochemistry (Supplementary Figure 2). The area represented by CD31+ vasculature increased from the small tumors imaged at Day 0 or 1 (~2–3 mm in diameter) to reach a peak for tumors imaged at Day 7 (~5–7 mm in diameter) and decreased again for larger tumors imaged at Day 14–21 (Supplementary Figure 2A–G. NRP expression on the vascular lumen was observed for tumors over the range of diameters of interest, including 3.2, 7.6 and 9.2 mm diameter tumors in Supplementary Figure 2H–J, respectively.

### Complement fixation

The fluorescently-tagged antibody to C3b bound to CRPPR-targeted microbubbles incubated in human serum but did not bind significantly to control (non-targeted microbubbles) or to either microbubble preparation incubated in saline (Fig. 6G).

## Discussion

NRP targeting with a CendR peptide, including a C-terminal arginine with a free carboxyl group, facilitated sensitive molecular imaging of tumor vasculature. Developing a molecular imaging agent with this CendR peptide is particularly important due to the potential for effective drug delivery; with such an agent the presence of the receptor can be easily assayed. Most importantly, CendR and iRGD peptides show the potential to facilitate the internalization of therapeutics. However, as shown in [11], the utility of this strategy is highly dependent on the NRP concentration on the target cell. Paoli *et al* [11] reported that 100-nm liposomes coated with a 0.16 mol% CRPPR peptide terminated with a free carboxyl group bind to and internalize into NRP-expressing cells, but not NRP-negative cells. Previous studies have also demonstrated that the same peptide sequence with an amide group at the C-terminus bound nonspecifically to both NRP-expressing and NRP-negative cells; however, internalization was not enhanced [9, 11]. Therefore, the development of an

imaging probe that can detect the NRP vascular surface receptor has high significance for effective personalized therapeutic delivery.

With a 1 mol% peptide concentration on the surface of the microbubbles, MBs with CRPPR and ATWLPPR (and with a free carboxyl group at the C-terminus) bound to NRP-expressing cells 32.8 and 17.6 times higher than non-targeted MBs, respectively. In this analysis, the kinetics of the accumulation of ultrasound contrast agents was quantified in a manner similar to nuclear medicine agents. Here, the intensity difference between the tumor and vessel was determined by the ratio of MB distribution in tumor (target) and vessel (background). The target-to-background ratio increased over time for CRP MBs, but not for ATW and NT MBs.

An earlier paper studying cRGD MBs reported that 80% of the initial signal intensity remained bound to tumors at 7 min post injection [31]. In this paper, 67% of the initial signal associated with CRP MBs remained bound at 8 min post injection, which was 8.0 and 4.5 times greater than ATW and NT MBs, respectively. Both studies indicate that molecular imaging with vascularly-targeted MBs has a high selectivity. MBs with $1.2 \times 10^5$ scVEGF ligands/bubble (MB mean diameter 2.5 ± 1 μm) [24] or $8.2 \pm 1.6 \times 10^5$ cRGD ligands/bubble (MB mean diameter 2.75 ± 0.02 μm) [31] have also been reported to effectively target tumor vasculature. With the area of one DSPC head group occupying ~0.65 $nm^2$ [33], the ligand concentrations on the MB membrane were calculated as 0.4% and 2.2% for scVEGF and cRGD, respectively, which is similar to the lipo-PEG-peptide percentage used in this paper (1%).

It has also been reported that multiple injections of targeted MBs within 60 minutes do not block sufficient binding sites to bias molecular imaging data [34], which allows for imaging sessions with consecutive targeted MB injections. However, insonation of targeted MBs can reduce blood flow for up to 40 minutes with a frequency of 5 MHz and peak-negative pressure of 2 or 4 MPa [20]. In this paper, we found that insonation of targeted MBs at 5 MHz and 1 MPa does not decrease blood flow or affect binding, which allowed us to compare different targeted MBs in four repeated injections.

Ideal characteristics of targeted contrast agents include a stable construct, highly selective targeting and low immunogenicity. Selective targeting is usually created by conjugating ligands, antibodies [14, 35–40] or short peptides [20, 24, 25, 31, 41–48] onto the surface of the contrast agent. Methods for conjugation include biological interaction (e.g., biotin-avidin [14, 20, 35–40, 44, 45]) and covalent bonds [24, 25, 31, 34, 42, 46–48]. The immunogenicity of short peptides is less than that of antibodies and is also reduced by covalent coupling rather than biotin-avidin interactions. Conjugation by covalent bonds can be accomplished either before or after microbubble formation, either by incorporating lipo-PEG-peptides or post-coupling with strategies such as maleimide-thiol interactions. The latter strategy requires a longer preparation time, which can affect stability [49]. Therefore, in this paper, lipo-PEG-peptide synthesis was used to create targeted MBs.

We have previously evaluated the attachment of C3/C3b and production of soluble C3a anaphylotoxin resulting from microbubbles that incorporate a surface conjugated ligand

[13]. In the previous study, microbubbles incorporating cyclic RGD within the lipo-PEG-peptide and microbubbles with conjugated biotin were evaluated for immunogenicity. We found that human C3/C3b bound to microbubbles with the RGD peptide or biotin on the surface. Finally, we have previously shown that the circulation time of linear peptides terminated in arginine is significantly shorter than liposomes bearing a cyclic RGD [27]. The microbubbles studied here are similar in architecture to [13] and we found that the CRPPR-conjugated agent will also bind C3/C3b. This effect is likely exaggerated in these studies as compared with human studies due to the relatively high dose of microbubbles administered and the number of injections used for the comparison studies in this paper. However, it is important to be aware of the potential biological effect.

The effect of repeated injections over a period of 21 days was studied, and we observed faster blood clearance and reduced binding of targeted MB on day 7, 14 and 21 after the first injection. The faster clearance could be due to the accelerated blood clearance (ABC) phenomenon, which has been observed after repeated injection of polyethylene glycol (PEG)-conjugated particles with a diameter of 50 to 800 nm. In the previous study, a second dose of PEGylated particles was rapidly cleared from circulation when administered within a limited time interval after the injection of the first dose due to enhanced accumulation in the liver [50]. Here, the rapid clearance of the contrast agent could also result from complement-mediated immunogenicity at the later time points as described above.

Due to the reduced circulation of the microbubbles, accumulation at the target site was expected to be reduced in the later studies and this was verified. Low MB binding at these later time points could also result from a reduction in the angiogenic vasculature at the later time points although we demonstrated that tumors in the size range for which the intensity had decreased (7 Day cohort with a diameter of ~7 mm) were highly vascular and did retain NRP staining on the vasculature. Given that NRP is present on both the vessel wall and tumor cells, accurate quantification and serial comparison of the luminal expression intensity as a function of time is not possible with immunohistochemistry. A decrease in microbubble accumulation as the tumor grows was also reported for VEGF2-targeted MBs, and changes in NRP expression may be a factor here as well [43].

Finally, in order to characterize the binding of MBs to cells *in vitro*, the number of bound MBs per field of view or per cell has often been studied in the literature [24, 51, 52]. However, considering that the affinity of MBs to cells also depends on MB size, which affects the number of available ligands, we chose to study the area covered with MBs, rather than number of MBs, per field of view. Computing binding based on area is superior to number also for the use of automatic recognition by image-analysis software, since targeted MBs can adhere to one another, which makes the automatic recognition of single MBs difficult.

## Conclusions

A molecular imaging agent capable of assessing the important NRP vascular target was synthesized and validated. Two lipo-PEG-peptides incorporating neuropilin-1 targeted peptides, CRPPR and ATWLPPR, were synthesized and used to form NRP-targeted

microbubbles that were successfully applied to imaging NRP concentrations on angiogenic vessels *in vivo*. CRPPR MBs also bound 2.6 and 15.6 times more than ATWLPPR MBs and non-targeted MBs *in vitro*, respectively, and binding was inhibited both *in vitro* and *in vivo* by pretreatment with an anti-NRP antibody. *In vivo*, we found that tumor echogenicity for the CRPPR-targeted MBs was 8.0 and 4.5 times higher than ATW and NT MBs and provided the opportunity to image small tumors with a high contrast-noise ratio. A set of parameters for MB destruction (5 MHz, 1 MPa, and 1 sec) was found to destroy >90% of the US MB signal, without significant effects on tumor blood flow or MB binding. Accelerated blood clearance and reduced MB binding were observed 7–21 days after the first injection.

## Supplementary Material

Refer to Web version on PubMed Central for supplementary material.

## Acknowledgments

The authors would thank Dr. X. W. Hu for thoughtful discussions. The support of NIHR01CA112356 and NIHR01CA134659 is gratefully acknowledged.

## References

1. Lindner JR. Microbubbles in medical imaging: current applications and future directions. Nat Rev Drug Discov. 2004; 3:527–32. [PubMed: 15173842]
2. Klibanov AL. Microbubble contrast agents - Targeted ultrasound imaging and ultrasound-assisted drug-delivery applications. Invest Radiol. 2006; 41:354–62. [PubMed: 16481920]
3. Panje CM, Wang DS, Willmann JK. Ultrasound and Microbubble-Mediated Gene Delivery in Cancer Progress and Perspectives. Invest Radiol. 2013; 48:755–69. [PubMed: 23697924]
4. Soker S, Takashima S, Miao HQ, Neufeld G, Klagsbrun M. Neuropilin-1 is expressed by endothelial and tumor cells as an isoform-specific receptor for vascular endothelial growth factor. Cell. 1998; 92:735– 45. [PubMed: 9529250]
5. Straume O, Akslen LA. Increased expression of VEGF-receptors (FLT-1, KDR, NRP-1) and thrombospondin-1 is associated with glomeruloid microvascular proliferation, an aggressive angiogenic phenotype, in malignant melanoma. Angiogenesis. 2003; 6:295–301. [PubMed: 15166498]
6. Broholm H, Laursen H. Vascular endothelial growth factor (VEGF) receptor neuropilin-1's distribution in astrocytic tumors. APMIS : acta pathologica, microbiologica, et immunologica Scandinavica. 2004; 112:257–63.
7. Stephenson JM, Banerjee S, Saxena NK, Cherian R, Banerjee SK. Neuropilin-1 is differentially expressed in myoepithelial cells and vascular smooth muscle cells in preneoplastic and neoplastic human breast: a possible marker for the progression of breast cancer. International journal of cancer Journal international du cancer. 2002; 101:409–14. [PubMed: 12216067]
8. Fakhari M, Pullirsch D, Abraham D, Paya K, Hofbauer R, Holzfeind P, et al. Selective upregulation of vascular endothelial growth factor receptors neuropilin-1 and -2 in human neuroblastoma. Cancer. 2002; 94:258–63. [PubMed: 11815985]
9. Teesalu T, Sugahara KN, Kotamraju VR, Ruoslahti E. C-end rule peptides mediate neuropilin-1-dependent cell, vascular, and tissue penetration. Proc Natl Acad Sci U S A. 2009; 106:16157–62. [PubMed: 19805273]
10. Starzec A, Vassy R, Martin A, Lecouvey M, Di Benedetto M, Crepin M, et al. Antiangiogenic and antitumor activities of peptide inhibiting the vascular endothelial growth factor binding to neuropilin-1. Life Sci. 2006; 79:2370–81. [PubMed: 16959272]

11. Paoli EE, Ingham ES, Zhang H, Mahakian LM, Fite BZ, Gagnon MK, et al. Accumulation, internalization and therapeutic efficacy of neuropilin-1-targeted liposomes. J Control Release. 2014; 178:108–17. [PubMed: 24434424]
12. Sugahara KN, Teesalu T, Karmali PP, Kotamraju VR, Agemy L, Girard OM, et al. Tissue-Penetrating Delivery of Compounds and Nanoparticles into Tumors. Cancer Cell. 2009; 16:510–20. [PubMed: 19962669]
13. Borden MA, Zhang H, Gillies RJ, Dayton PA, Ferrara KW. A stimulus-responsive contrast agent for ultrasound molecular imaging. Biomaterials. 2008; 29:597–606. [PubMed: 17977595]
14. Lutz AM, Bachawal SV, Drescher CW, Pysz MA, Willmann JK, Gambhir SS. Ultrasound Molecular Imaging in a Human CD276 Expression-Modulated Murine Ovarian Cancer Model. Clin Cancer Res. 2014; 20:1313–22. [PubMed: 24389327]
15. Deshpande N, Ren Y, Foygel K, Rosenberg J, Willmann JK. Tumor Angiogenic Marker Expression Levels during Tumor Growth: Longitudinal Assessment with Molecularly Targeted Microbubbles and US Imaging. Radiology. 2011; 258:804–11. [PubMed: 21339349]
16. Palmowski M, Huppert J, Ladewig G, Hauff P, Reinhardt M, Mueller MM, et al. Molecular profiling of angiogenesis with targeted ultrasound imaging: early assessment of antiangiogenic therapy effects. Mol Cancer Ther. 2008; 7:101–9. [PubMed: 18202013]
17. Weissleder, R.; Ross, BD.; Rehemtulla, A.; Gambhir, SS. Molecular Imaging: Principles and Practice. People's Medical Publishing House-USA; 2010.
18. Zhang XZ, Xiong ZM, Wu Y, Cai WB, Tseng JR, Gambhir SS, et al. Quantitative PET imaging of tumor integrin alpha(v)beta(3) expression with F-18-FRGD2. J Nucl Med. 2006; 47:113–21. [PubMed: 16391195]
19. Logan J. Graphical analysis of PET data applied to reversible and irreversible tracers. Nucl Med Biol. 2000; 27:661–70. [PubMed: 11091109]
20. Hu XW, Kheirolomoom A, Mahakian LM, Beegle JR, Kruse DE, Lam KS, et al. Insonation of Targeted Microbubbles Produces Regions of Reduced Blood Flow Within Tumor Vasculature. Invest Radiol. 2012; 47:398–405. [PubMed: 22659591]
21. Stieger SM, Caskey CF, Adamson RH, Qin SP, Curry FRE, Wisner ER, et al. Enhancement of vascular permeability with low-frequency contrast-enhanced ultrasound in the chorioallantoic membrane model. Radiology. 2007; 243:112–21. [PubMed: 17392250]
22. Skyba DM, Price RJ, Linka AZ, Skalak TC, Kaul S. Direct in vivo visualization of intravascular destruction of microbubbles by ultrasound and its local effects on tissue. Circulation. 1998; 98:290–3. [PubMed: 9711932]
23. Price RJ, Skyba DM, Kaul S, Skalak TC. Delivery of colloidal, particles and red blood cells to tissue through microvessel ruptures created by targeted microbubble destruction with ultrasound. Circulation. 1998; 98:1264–7. [PubMed: 9751673]
24. Anderson CR, Rychak JJ, Backer M, Backer J, Ley K, Klibanov AL. scVEGF Microbubble Ultrasound Contrast Agents A Novel Probe for Ultrasound Molecular Imaging of Tumor Angiogenesis. Invest Radiol. 2010; 45:579–85. [PubMed: 20733505]
25. Bzyl J, Lederle W, Rix A, Grouls C, Tardy I, Pochon S, et al. Molecular and functional ultrasound imaging in differently aggressive breast cancer xenografts using two novel ultrasound contrast agents (BR55 and BR38). Eur Radiol. 2011; 21:1988–95. [PubMed: 21562807]
26. Chan, WC.; White, PD. Fmoc solid phase peptide synthesis : a practical approach. New York: Oxford University Press; 2000.
27. Zhang H, Kusunose J, Kheirolomoom A, Seo JW, Qi JY, Watson KD, et al. Dynamic imaging of arginine-rich heart-targeted vehicles in a mouse model. Biomaterials. 2008; 29:1976–88. [PubMed: 18255141]
28. Feshitan JA, Chen CC, Kwan JJ, Borden MA. Microbubble size isolation by differential centrifugation. J Colloid Interface Sci. 2009; 329:316–24. [PubMed: 18950786]
29. Stieger SM, Dayton PA, Borden MA, Caskey CF, Griffey SM, Wisner ER, et al. Imaging of angiogenesis using Cadence (TM) contrast pulse sequencing and targeted contrast agents. Contrast Media Mol Imaging. 2008; 3:9–18. [PubMed: 18335479]
30. Cardiff RDHN, Engelberg JA, Munn RJ, Miller CH, Walls JE, Chen JQ, Velásquez-García HA, Galvez JJ, Bell KJ, Beckett LA, Li YJ, Borowsky AD. Quantitation of fixative-induced

morphologic and antigenic variation in mouse and human breast cancers. Laboratory Investigation. 2013; 93:480–97. [PubMed: 23399853]

31. Anderson CR, Hu XW, Zhang H, Tlaxca J, Decleves AE, Houghtaling R, et al. Ultrasound Molecular Imaging of Tumor Angiogenesis With an Integrin Targeted Microbubble Contrast Agent. Invest Radiol. 2011; 46:215–24. [PubMed: 21343825]
32. Stieger SM, Dayton PA, Borden MA, Caskey CF, Griffey SM, Wisner ER, et al. Imaging of angiogenesis using Cadence™ contrast pulse sequencing and targeted contrast agents. Contrast Media & Molecular Imaging. 2008; 3:9–18. [PubMed: 18335479]
33. Petrache HI, Dodd SW, Brown MF. Area per Lipid and Acyl Length Distributions in Fluid Phosphatidylcholines Determined by 2H NMR Spectroscopy. Biophysical Journal. 2000; 79:3172–92. [PubMed: 11106622]
34. Streeter JE, Dayton PA. An In Vivo Evaluation of the Effect of Repeated Administration and Clearance of Targeted Contrast Agents on Molecular Imaging Signal Enhancement. Theranostics. 2013; 3:93–8. [PubMed: 23424189]
35. Wu ZJ, Curaj A, Fokong S, Liehn EA, Weber C, Lammers T, et al. Rhodamine-Loaded Intercellular Adhesion Molecule-1-targeted Microbubbles for Dual-Modality Imaging Under Controlled Shear Stresses. Circ-Cardiovasc Imaging. 2013; 6:974–81. [PubMed: 24036383]
36. Tlaxca JL, Rychak JJ, Ernst PB, Konkalmatt PR, Shevchenko TI, Pizzaro TT, et al. Ultrasound-based molecular imaging and specific gene delivery to mesenteric vasculature by endothelial adhesion molecule targeted microbubbles in a mouse model of Crohn's disease. J Control Release. 2013; 165:216– 25. [PubMed: 23142578]
37. Warram JM, Sorace AG, Saini R, Borovjagin AV, Hoyt K, Zinn KR. Systemic delivery of a breast cancer-detecting adenovirus using targeted microbubbles. Cancer Gene Ther. 2012; 19:545–52. [PubMed: 22653385]
38. Sorace AG, Saini R, Mahoney M, Hoyt K. Molecular Ultrasound Imaging Using a Targeted Contrast Agent for Assessing Early Tumor Response to Antiangiogenic Therapy. J Ultrasound Med. 2012; 31:1543– 50. [PubMed: 23011617]
39. Warram JM, Sorace AG, Saini R, Umphrey HR, Zinn KR, Hoyt K. A Triple-Targeted Ultrasound Contrast Agent Provides Improved Localization to Tumor Vasculature. J Ultrasound Med. 2011; 30:921– 31. [PubMed: 21705725]
40. Ferrante EA, Pickard JE, Rychak J, Klibanov A, Ley K. Dual targeting improves microbubble contrast agent adhesion to VCAM-1 and P-selectin under flow. J Control Release. 2009; 140:100–7. [PubMed: 19666063]
41. Marinelli S, Salvatore V, Toaldo MB, Milazzo M, Croci L, Venerandi L, et al. Evaluation of the impact of transient interruption of antiangiogenic treatment using ultrasound-based techniques in a murine model of hepatocellular carcinoma. BMC Cancer. 2014:14. [PubMed: 24410891]
42. Fokong S, Fragoso A, Rix A, Curaj A, Wu ZJ, Lederle W, et al. Ultrasound Molecular Imaging of E-Selectin in Tumor Vessels Using Poly n-Butyl Cyanoacrylate Microbubbles Covalently Coupled to a Short Targeting Peptide. Invest Radiol. 2013; 48:843–50. [PubMed: 23857137]
43. Bzyl J, Palmowski M, Rix A, Arns S, Hyvelin JM, Pochon S, et al. The high angiogenic activity in very early breast cancer enables reliable imaging with VEGFR2-targeted microbubbles (BR55). Eur Radiol. 2013; 23:468–75. [PubMed: 22878592]
44. Yan F, Li XA, Jin QF, Jiang CX, Zhang ZD, Ling T, et al. Therapeutic ultrasonic microbbles carrying paclitaxel and LyP-1 peptide: Preparation, characterization and application to ultrasound-assisted chemotherapy in breast cancer cells. Ultrasound in Medicine and Biology. 2011; 37:768–79. [PubMed: 21458148]
45. Willmann JK, Kimura RH, Deshpande N, Lutz AM, Cochran JR, Gambhir SS. Targeted Contrast-Enhanced Ultrasound Imaging of Tumor Angiogenesis with Contrast Microbubbles Conjugated to Integrin-Binding Knottin Peptides. J Nucl Med. 2010; 51:433–40. [PubMed: 20150258]
46. Streeter JE, Gessner R, Miles I, Dayton PA. Improving Sensitivity in Ultrasound Molecular Imaging by Tailoring Contrast Agent Size Distribution: In Vivo Studies. Mol Imaging. 2010; 9:87–95. [PubMed: 20236606]

47. Pochon S, Tardy I, Bussat P, Bettinger T, Brochot J, von Wronski M, et al. BR55: A Lipopeptide-Based VEGFR2-Targeted Ultrasound Contrast Agent for Molecular Imaging of Angiogenesis. Invest Radiol. 2010; 45:89–95. [PubMed: 20027118]

48. Pillai R, Marinelli ER, Fan H, Nanjappan P, Song B, von Wronski MA, et al. A Phospholipid-PEG2000 Conjugate of a Vascular Endothelial Growth Factor Receptor 2 (VEGFR2)-Targeting Heterodimer Peptide for Contrast-Enhanced Ultrasound Imaging of Angiogenesis. Bioconjugate Chem. 2010; 21:556–62.

49. Kwan JJ, Borden MA. Microbubble Dissolution in a Multigas Environment. Langmuir. 2010; 26:6542–8. [PubMed: 20067292]

50. Abu Lila AS, Kiwada H, Ishida T. The accelerated blood clearance (ABC) phenomenon: Clinical challenge and approaches to manage. J Control Release. 2013; 172:38–47. [PubMed: 23933235]

51. Dayton PA, Pearson D, Clark J, Simon S, Schumann PA, Zutshi R, et al. Ultrasonic Analysis of Peptide- and Antibody-Targeted Microbubble Contrast Agents for Molecular Imaging of alpha(V)beta(3)-Expressing Cells. Mol Imaging. 2004; 3:125–34. [PubMed: 15296677]

52. Weller GER, Wong MKK, Modzelewski RA, Lu EX, Klibanov AL, Wagner WR, et al. Ultrasonic imaging of tumor angiogenesis using contrast microbubbles targeted via the tumor-binding peptide arginin-arginine-leucine. Cancer Research. 2005; 65:533–9. [PubMed: 15695396]

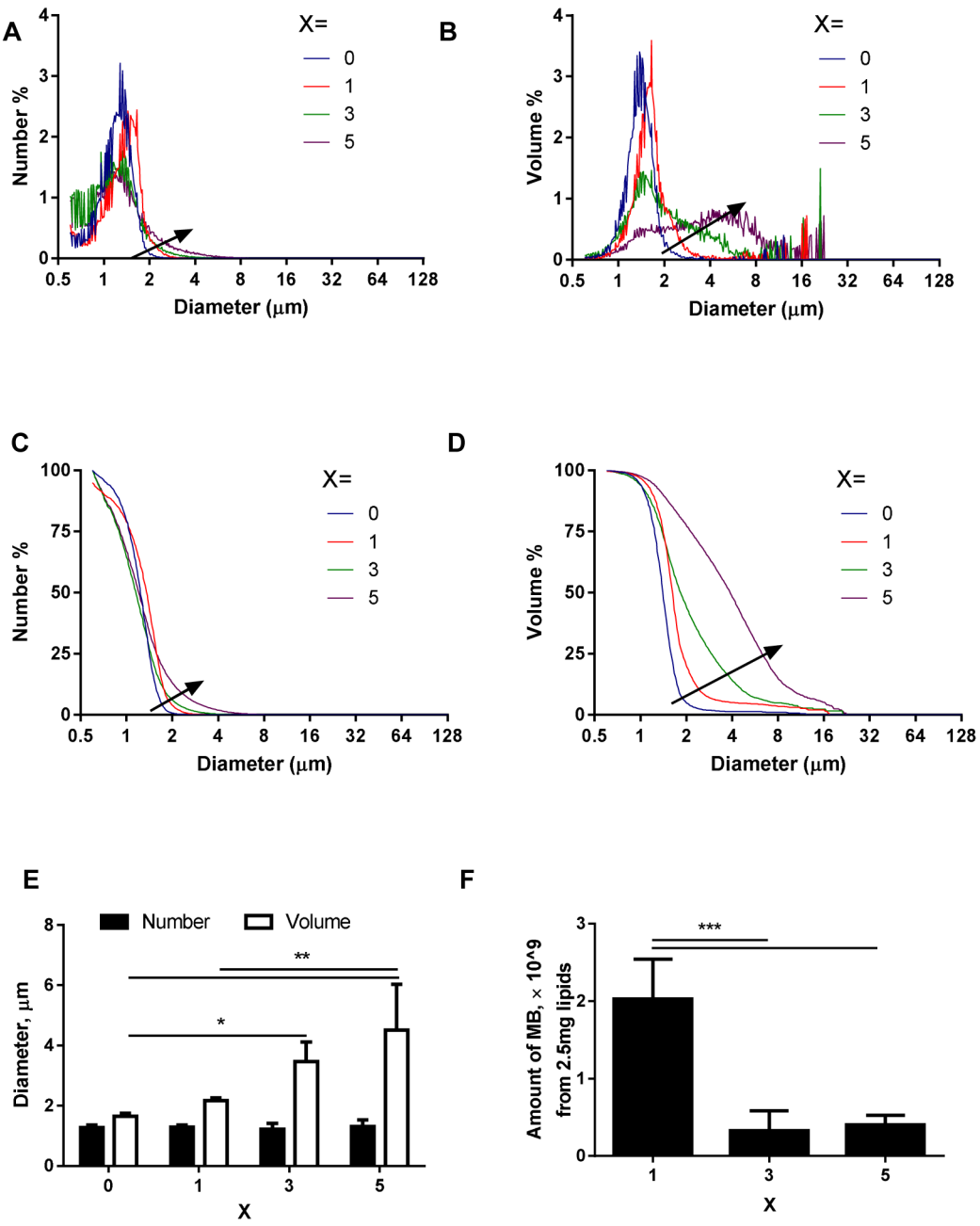


**FIGURE 1.**

Typical size distribution curves (A–D), mean diameters (E), and amount (F) of MBs produced from lipid formulations with different ligand percentages, X. MB lipid formulation was DSPC:DSPE-PEG2k:CRPPR-LPP = 90:10-X:X (mol/mol/mol). A) number-weighted size distribution; B) volume-weighted size distribution; C) number-weighted cumulative size distribution; D) volume-weighted cumulative size distribution; E) the mean diameter of MBs; with X = 0,1,3,5; F) the total amount of MBs obtained from 2.5 mg of lipids. For each recipe, n=4. The arrow points in the direction of increasing CRP percentage. An increase in ligand incorporation from 1 to 5 mol% increased the number of large-sized MBs (3–10 μm),

and decreased the total volume of MBs produced from 2.5 mg lipids, therefore, the ligand percentage, X, was set as 1 for the rest of this paper. One-way ANOVA with Tukey's multiple comparisons correction was performed to test significance: *, $p<0.05$; **, $p<0.01$; ***, $p<0.001$.

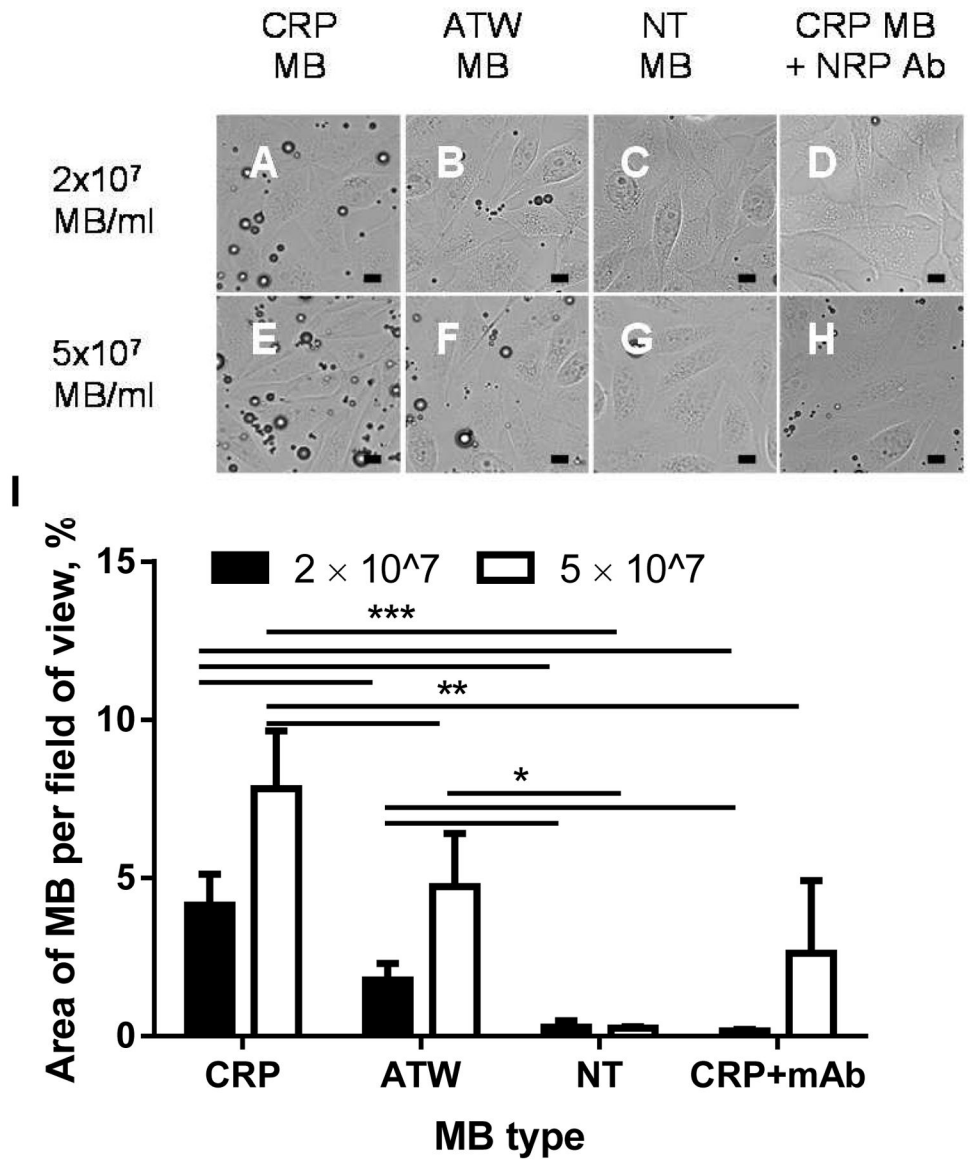


**FIGURE 2.**

Microscopic images (A–H) and quantification results (I) for PPC-1 cells treated with CRP MBs (A and E), ATW MBs (B and F), NT MBs (C and G), and NRP antibody followed with CRP MBs (D and H), at $2 \times 10^7$ MB/ml (A–D) or $5 \times 10^7$ MB/ml (E–H). I) Quantification of the area of bound microbubbles. CRP MBs bound 2.6 and 15.6 ($2 \times 10^7$ MBs/ml), 1.9 and 32.8 ($5 \times 10^7$ MBs/ml), times more than ATW MBs and NT MBs, respectively, and binding was inhibited to 4% ($2 \times 10^7$ MBs/ml) and 39% ($5 \times 10^7$ MBs/ml) by incubating the cells with the NRP-1 antibody before adding the NRP MB suspension. For each recipe, n=4–5. One-way ANOVA with Tukey's multiple comparisons correction was performed (GraphPad Prism 6) to test the significance: *, $p<0.05$; **, $p<0.01$; ***, $p<0.001$. The scale bar is 10 μm.

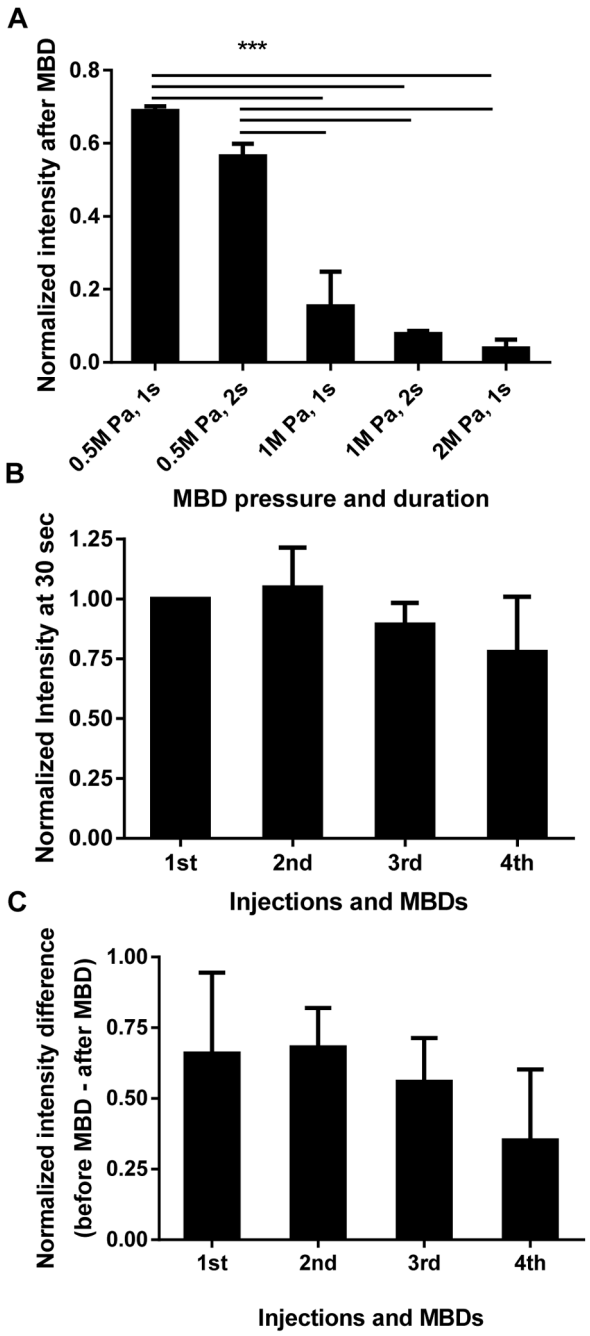


**FIGURE 3.**

The optimization of MBD parameters. A) The US signal intensity after MBD was normalized by the US signal intensity before MBD and plotted as a function of MBD pressure and duration, n=3. B) The effect of repeated injection/MBDs on blood flow, characterized by the signal intensity at 30 sec post injection, normalized by the value from the first injection; C) The effect of repeated injection/MBD on MB binding, characterized by the tumor intensity change caused by MBD, normalized by the tumor intensity at 30 sec post injection, n=3. MBD with 1 MPa for 1 sec destroyed most of the MB signal (A), while not

significantly affecting blood flow (B), and not significantly affecting the CRP MB binding (C). Paired one-way ANOVA with Dunnett's multiple comparisons correction was performed to test the significance between the first and the later injections. *, $p<0.05$; **, $p<0.01$; ***, $p<0.001$.

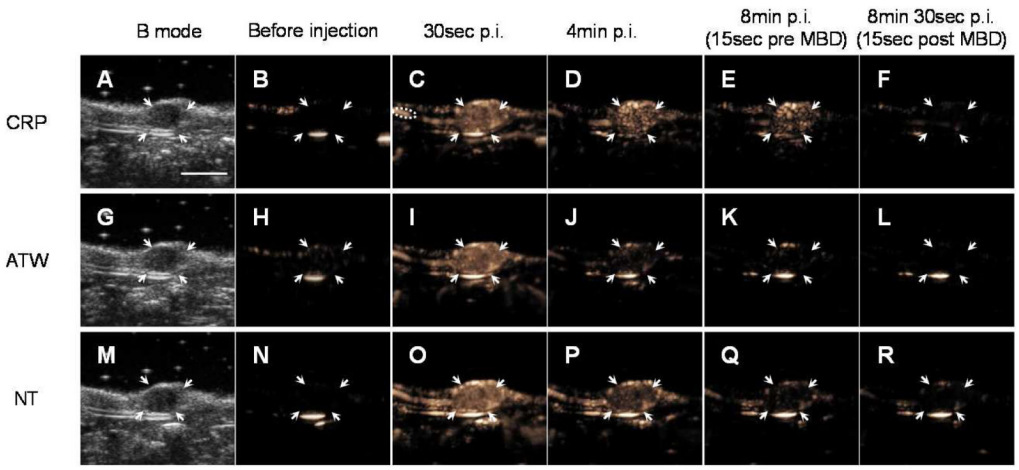


**FIGURE 4.**

One example set of images showing the binding kinetics and blood clearance of CRP (first row, A–F), ATW (second row, G–L), and NT (third row, M–R) MBs. For each tumor, $5 \times 10^7$ CRP, ATW, and NT MBs were injected consecutively with a random order. One B mode image (first column, A, G, M) was acquired before injection to define the tumor area, and 10 sec CPS clips were recorded and averaged before injection (B, H, N), 0, 0.5 (C, I, O), 1, 2, 4 (D, J, P), 6, 8 (E, K, Q), 8.25, and 8.5 (F, L, R) min after injection. MBD was applied at 8.25 min after injection. Orange pixels represent CPS enhancement (the presence of the microbubbles in the imaging plane). Regions of interest are indicated as follows: arrows indicate tumor; and dashed circle (C) indicates a nearby blood vessel used to assess MB circulation. The scale bar (A) represents 5 mm.

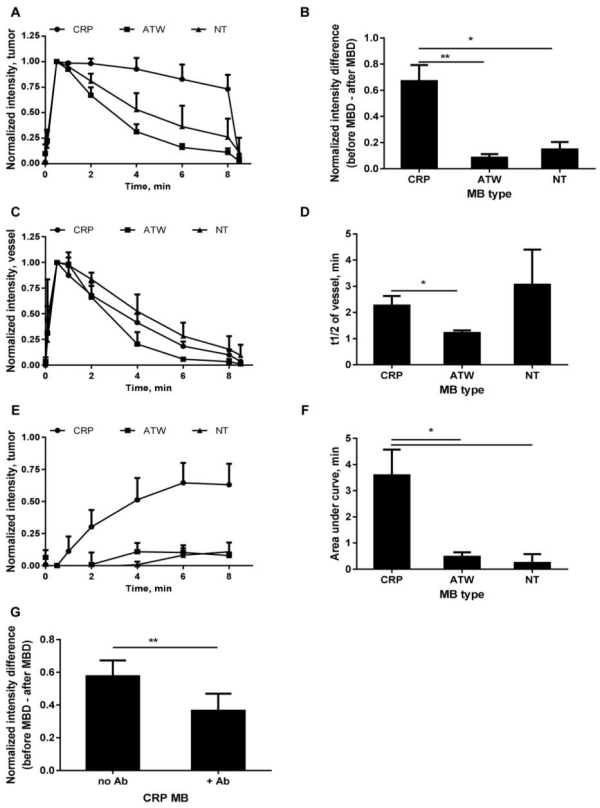


**FIGURE 5.**

*In vivo* summary of CRP, ATW and NT MB performance in the imaging of tumors (A and B), blood vessels (C and D), tumor – vessel comparison (E and F), and antibody blocking of CRP MB tumor accumulation (G). Normalized intensities in tumors decreased more slowly with CRP MBs than with ATW and NT MBs (A), indicating that the CRP MBs bound to the tumor more than ATW and NT MBs (B). The blood clearance of CRP MBs was similar to NT MBs, and slower than ATW MBs (C), with half-lives of 2.2, 1.2, and 3.1 min for CRP, ATW, and NT MBs, respectively (D). The normalized intensity difference between the tumor and vessel shows that the target/background signal ratio increased with CRP MBs, but not with ATW or NT MBs (E and F). Antibody injection decreased the normalized intensity difference from 0.58 ± 0.10 to 0.36 ± 0.10 (G). For (A–F), n=4, paired one way ANOVA tests with Tukey's multiple comparisons correction were performed in Graphpad Prism 6; and for G, n=7, a paired t test was performed in Excel. *, $p<0.05$; **, $p<0.01$.

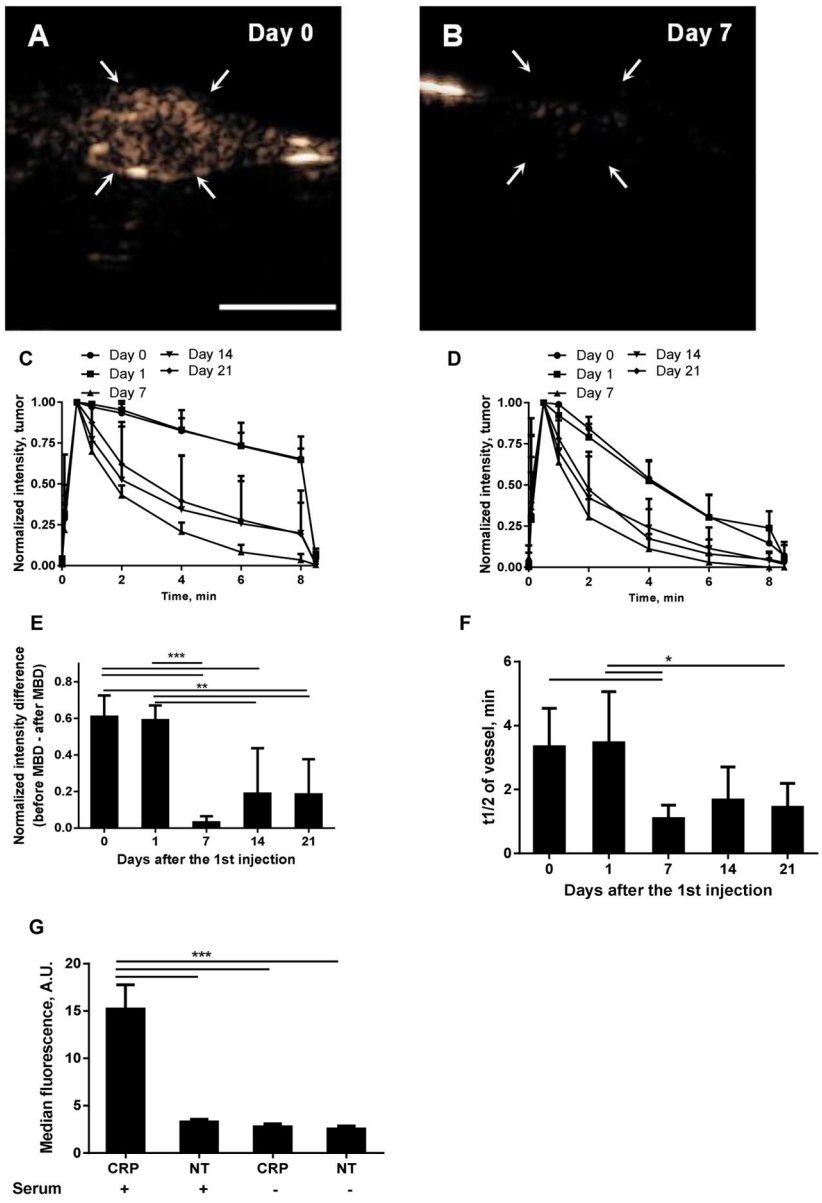


**FIGURE 6.**

The effect of repeated CRP MB injections over a duration of 21 days: A–B) CPS images at 8 min after CRP MB injection on Day 0 (the first injection, A), and Day 7 (B); C–D) signal kinetics in tumor (C) and vessel (D) and E–F) normalized signal intensity change caused by MBD (E), and blood clearance half-lives (F), after CRP MB injections at Day 0, 1, 7, 14, and 21. G) Fluorescence intensity resulting from a fluorescently-tagged antibody to C3b which accumulates on CRP-conjugated but not non-targeted (NT) microbubbles. Compared to Day 0 and Day 1, the clearance from the circulation was faster and the accumulation on Day 7, 14, and 21 was reduced. n = 5–6 for each condition. The scale bar (A) represents 5 mm. One-way ANOVA tests with Tukey's multiple comparisons correction were performed in Graphpad Prism 6, *, $p<0.05$; **, $p<0.01$; ***, $p<0.001$.